Electronic Supplementary Information (ESI)

Bringing 5-(3,4-dicarboxylphenyl)picolinic acid to crystal engineering research: Hydrothermal assembly, structural features, and photocatalytic activity of Mn, Ni, Cu, and Zn coordination polymers

Jin-Zhong Gu [a,*], Yan Cai [a], Xiao-Xiao Liang [a], Jiang Wu [a], Zi-Fa Shi [a], Alexander M. Kirillov [b,*]

[a]Key Laboratory of Nonferrous Metal Chemistry and Resources Utilization of Gansu Province, State Key Laboratory of Applied Organic Chemistry and College of Chemistry and Chemical Engineering, Lanzhou University, Lanzhou, 730000 (P. R. China)

[b]Centro de Química Estrutural, Instituto Superior Técnico, Universidade de Lisboa, Av. Rovisco Pais, 1049-001, Lisbon, Portugal

Fax: (+86) 931-891-5196
E-mail: gujzh@lzu.edu.cn; kirillov@tecnico.ulisboa.pt

Synthesis and analytical data for 2–7

Synthesis of {[Mn(μ-Hdppa)(2,2′-H_2biim)(H_2O)]·H_2O}$_n$ (2). A mixture of $MnCl_2·4H_2O$ (59.4 mg, 0.30 mmol), H_3dppa (86.1 mg, 0.30 mmol), 2,2′-H_2biim (40.2 mg, 0.3 mmol), NaOH (24 mg, 0.60 mmol), and H_2O (10 mL) was stirred at room temperature for 15 min, then sealed in a 25 mL Teflon-lined stainless steel vessel, and heated at 160 °C for 3 days, followed by cooling to room temperature at a rate of 10 °C·h^{-1}. Yellow block-shaped crystals of **2** were isolated manually, washed with distilled water, and dried (yield 60% based on H_3dppa). Anal. Calcd for $C_{20}H_{17}MnN_5O_8$: C, 47.07; H, 3.36; N, 13.72. Found: C, 47.33; H, 3.38; N, 13.49%. IR (KBr, cm^{-1}): 3369 m, 3010 w, 1684 m, 1622 s, 1597 m, 1560 s, 1430 m, 1399 m, 1362 s, 1262 m, 1163 w, 1114 m, 1027 w, 990 w, 922 w, 879 w, 791 m, 755 w, 693 m, 649 w, 569 w.

Synthesis of [Ni(Hdppa)(phen)$_2$]·4H_2O (3). A mixture of $NiCl_2·6H_2O$ (71.3 mg, 0.3 mmol), H_3dppa (86.0 mg, 0.3 mmol), phen (60.0 mg, 0.30 mmol), NaOH (24.0 mg, 0.60 mmol), and H_2O (10 mL) was stirred at room temperature for 15 min, then sealed in a 25 mL Teflon-lined stainless steel vessel, and heated at 160 °C for 3 days, followed by cooling to room temperature at a rate of 10 °C·h^{-1}. Purple block-shaped crystals of **3** were isolated manually, washed with distilled water and dried (yield 62% based on H_3dppa). Anal. Calcd for $C_{38}H_{31}NiN_5O_{10}$: C, 58.79; H, 4.02; N, 9.02. Found: C, 58.51; H, 4.00; N, 9.10%. IR (KBr, cm^{-1}): 3359 w, 3065 w, 1634 w, 1591 m, 1516 m, 1428 m, 1352 s, 1253 w, 1170 w, 1101 w, 1039 w, 851 m, 769 w, 719 m, 694 w, 644 w, 536 w.

Synthesis of {[Ni(μ-Hdppa)(μ-4,4′-bipy)(H_2O)]·H_2O}$_n$ (4). A mixture of $NiCl_2·6H_2O$ (71.3 mg, 0.30 mmol), H_3dppa (86.1 mg, 0.30 mmol), 4,4′-bipy (46.8 mg, 0.30 mmol), NaOH (24.0 mg, 0.60 mmol), and H_2O (10 mL) was stirred at room temperature for 15 min, then sealed in a 25 mL Teflon-lined stainless steel vessel, and heated at 160 °C for 3 days, followed by cooling to room temperature at a rate of 10 °C·h^{-1}. Purple block-shaped crystals of **4** were isolated manually, washed with distilled water and dried (yield 68% based on H_3dppa). Anal. Calcd for $C_{24}H_{19}NiN_3O_8$: C, 53.77; H, 3.57; N, 7.84. Found: C, 53.98; H, 3.56; N, 7.81%. IR (KBr, cm^{-1}): 3332 w, 3035 w, 1647 w, 1610 s, 1591 s, 1535 m, 1411 s, 1355 s, 1293 w, 1257 w, 1213 w, 1071 w, 1033 w, 1016 w, 922 w, 861 m, 817 m, 774

m, 737 w, 712 w, 637 m, 606 w, 520 w.

Synthesis of {[Cu_3(μ$_3$-dppa)(μ-Hdppa)(phen)$_4$][Cu(μ-Hdppa)$_2$]·10H_2O}$_n$ (5). A mixture of $CuCl_2·2H_2O$ (51.1 mg, 0.30 mmol), H_3dppa (86.1 mg, 0.30 mmol), phen (60.0 mg, 0.30 mmol), NaOH (24.0 mg, 0.60 mmol), and H_2O (10 mL) was stirred at room temperature for 15 min, then sealed in a 25 mL Teflon-lined stainless steel vessel, and heated at 160 °C for 3 days, followed by cooling to room temperature at a rate of 10 °C·h^{-1}. Blue block-shaped crystals of **5** were obtained (yield 40% based on H_3dppa). Anal. Calcd for $C_{180}H_{124}Cu_7N_{22}O_{46}$: C, 57.26; H, 3.31; N, 8.16. Found: C, 57.02; H, 3.33; N, 8.07. IR (KBr, cm^{-1}): 3648 w, 3302 w, 1660 m, 1578 m, 1509 m, 1428 m, 1340 s, 1296 w, 1253 w, 1220 w, 1177 w, 1139 w, 1101 w, 1045 w, 920 w, 851 m, 800 w, 769 w, 725 m, 687 w, 649 w, 593 w.

Synthesis of {[Ni_3(μ-dppa)$_2$(μ-1,4-bpb)$_2$(H_2O)$_6$]·4H_2O}$_n$ (6). A mixture of $NiCl_2·6H_2O$ (71.3 mg, 0.30 mmol), H_3dppa (57.4 mg, 0.20 mmol), 1,4′-bpb (69.8 mg, 0.30 mmol), NaOH (24.0 mg, 0.60 mmol), and H_2O (10 mL) was stirred at room temperature for 15 min, then sealed in a 25 mL Teflon-lined stainless steel vessel, and heated at 160 °C for 3 days, followed by cooling to room temperature at a rate of 10 °C·h^{-1}. Green block-shaped crystals of **6** were isolated manually, washed with distilled water and dried (yield 62% based on H_3dppa). Anal. Calcd for $C_{60}H_{56}Ni_3N_6O_{22}$: C, 51.87; H, 4.06; N, 6.05. Found: C, 51.59; H, 4.02; N, 6.02%. IR (KBr, cm^{-1}): 3425 m, 3134 w, 1603 s, 1572 m, 1548 w, 1486 w, 1386 s, 1306 w, 1244 w, 1220 w, 1164 w, 1071 w, 1034 w, 934 w, 897 w, 861 w, 841 w, 810 m, 761 w, 724 w, 693 w, 655 w, 550 w.

Synthesis of {[Zn_3(μ$_3$-dppa)$_2$(phen)$_2$(H_2O)$_2$]·4H_2O}$_n$ (7). A mixture of $ZnCl_2$ (40.9 mg, 0.30 mmol), H_3dppa (57.4 mg, 0.20 mmol), phen (60.0 mg, 0.30 mmol), NaOH (24.0 mg, 0.60 mmol), and H_2O (10 mL) was stirred at room temperature for 15 min, then sealed in a 25 mL Teflon-lined stainless steel vessel, and heated at 160 °C for 3 days, followed by cooling to room temperature at a rate of 10 °C·h^{-1}. Colorless block-shaped crystals of **7** were obtained (yield 60% based on H_3dppa). Anal. Calcd for $C_{52}H_{40}Zn_3N_6O_{18}$: C, 50.65; H, 3.27; N, 6.82. Found: C, 50.87; H, 3.29; N, 6.93. IR (KBr, cm^{-1}): 3441 w, 3071 w, 1603 s, 1521 m, 1428 m, 1378 s, 1296 w, 1258 w, 1159 w, 1089 w, 1032 w, 964 w, 901 w, 851 m, 826 m, 800 m, 725 m, 668 w, 574 w.

Magnetic properties

For manganese(II) and nickel(II) containing products **1**, **2**, **4**, and **6**, magnetic properties were also investigated. The variable-temperature magnetic susceptibilities were recorded on microcrystalline samples in the 2–300 K interval (Fig. S14). For the manganese(II) dimer **1** (Fig. 12), the $\chi_M T$ value of 4.40 $cm^3 \cdot mol^{-1} \cdot K$ at ambient temperature approaches the value (4.38 $cm^3 \cdot mol^{-1} \cdot K$) corresponding to one magnetically isolated high-spin manganese(II) ion (S_{Mn} = 5/2, g = 2.0). A decrease of the temperature leads to the gradual increase of the $\chi_M T$ values, which reach a dispersed maxmum of 4.45 $cm^3 \cdot mol^{-1} \cdot K$ at 21 K. After this temperature, $\chi_M T$ abruptly decreases to 4.10 $cm^3 \cdot mol^{-1} \cdot K$ at 2 K. In the 2–300 K range, the magnetic susceptibilities can be fitted to Curie-Weiss law with C = 4.46 $cm^3 \cdot mol^{-1} \cdot K$ and θ = –4.40 K. These data indicate a weak antiferromagnetic interaction within two adjacent Mn(II) centers. We attempted to fit the obtained magnetic data for **1** by applying an expression[1] for a dimanganese(II) unit: $H = -JS_1S_2$. Here, N, k, and β constants have their usual meaning. $\chi = 2Ng^2\beta^2A / KTB$ where:

$A = \exp(J/kT) + 5\exp(3J/kT) + 14\exp(6J/kT) + 30\exp(10J/kT) + 55\exp(15J/kT)$

$B = 1 + 3\exp(J/kT) + 5\exp(3J/kT) + 7\exp(6J/kT) + 9\exp(10J/kT) + 11\exp(15J/kT)$

The best fitting gives J = –2.34 cm^{-1}, g = 2.05, and $R = 4.04 \times 10^{-5}$. A negative J value confirms a weak antiferromagnetic coupling between two neighboring manganese(II) atoms.

For the 1D Mn(II) polymer **2**, the room temperature value of $\chi_M T$, 4.67 $cm^3 \cdot mol^{-1} \cdot K$, is slightly larger than the value (4.38 $cm^3 \cdot mol^{-1} \cdot K$) expected for a magnetically isolated high-spin Mn(II) ion (S = 5/2, g = 2.0). If temperature is lowered, the $\chi_M T$ values decrease continuously to a minimum of 2.01 $cm^3 \cdot mol^{-1} \cdot K$ at 2.0 K. Between 2 and 300 K, the magnetic susceptibility can be fitted to the Curie–Weiss law with C = 4.74 $cm^3 \cdot mol^{-1} \cdot K$ and θ = –6.27 K. These results also indicate an antiferromagnetic interaction between the adjacent Mn(II) centers. We attempted to fit the data for **2** by applying the following expression[2–4] for a 1D Mn(II) chain:

$H = -JS_iS_j$

$\chi_{chain} = (Ng^2\beta^2/kT)[A + Bx^2][1 + Cx + Dx^3]^{-1}$

with A = 2.9167, B = 208.04, C = 15.543, D = 2707.2, and $x = |J|/kT$

The susceptibility for **2** was simulated using this rough model, and resulting in J = –0.87 cm^{-1}, g = 2.03, and $R = 3.29 \times 10^{-5}$. A negative J parameter indicates a weak antiferromagnetic exchange coupling between the adjacent Mn(II) centers in **2**, which is in agreement with a negative θ value.

For **4**, the room temperature value of $\chi_M T$, 1.01 cm^3·mol^{-1}·K, is close to that of 1.00 cm^3·mol^{-1}·K expected for one magnetically isolated high-spin Ni(II) ion (S = 1, g = 2.0). The $\chi_M T$ values increase slowly on lowering the temperature until about 50 K, and then increase quickly to 1.70 cm^3·mol^{-1}·K at 2.0 K. Between 2 and 300 K, the magnetic susceptibilities can be fitted to the Curie-Weiss law with C = 1.03 cm^3·mol^{-1}·K and θ = 3.45 K. These results indicate a ferromagnetic interaction between the adjacent Ni(II) centers in compound **4**. An empirical (Weng's) formula can be applied to analyze the 1D systems with S = 1, using numerical procedures;[4,5]

$$H = -JS_iS_j$$

$$\chi_M = \frac{N\beta^2 g^2}{kT}\frac{A}{B}$$

$$A = 2.0 + 0.0194x + 0.777x^2$$

$$B = 3.0 + 4.346x + 3.232x^2 + 5.834x^2$$

with $x = |J|/kT$

Using this method, the best-fit parameters for **4** were obtained: J = 2.93 cm^{-1}, g = 2.03 and $R = 2.57 \times 10^{-5}$. A positive J parameter indicates a weak ferromagnetic exchange coupling between the adjacent Ni(II) centers in **4**, which is in agreement with a positive θ value. According to the structure of **4** (Fig. 4b), there is one magnetic exchange pathway within the chain through one *syn-anti* carboxylate bridge, which can be responsible for the observed ferromagnetic exchange.

As shown in Fig. 12, the room temperature value of $\chi_M T$ for **6**, 3.15 cm^3·mol^{-1}·K, is close to the value (3.00 cm^3·mol^{-1}·K) expected for three magnetically isolated high-spin Ni(II) ions (S = 1, g = 2.0). By decreasing the temperature, the $\chi_M T$ values slowly decline until about 20 K and then decrease quickly to 2.00 cm^3·mol^{-1}·K at 2.0 K. Between 2 and 300 K, the magnetic susceptibility can be fitted to the Curie–Weiss law with C = 3.15 cm^3·mol^{-1}·K and θ = –3.74 K. These results

indicate an antiferromagnetic interaction between the adjacent Ni(II) centers. Because of the long metal-metal separation between the Ni_2 (Ni1/Ni1i) and the third Ni2 atom (Fig. 6), only the coupling interactions within the dinickel(II) units are considered. We tried to fit the magnetic data of **6** by applying the following expression[6] for a dinuclear Ni(II) unit:

$$H = -JS_1S_2$$

$$\chi_{M'} = \frac{N\beta^2 g^2}{3k(T-\theta)} \frac{\sum S'(S'+1)(2S'+1)e^{-E(S')/kT}}{\sum (2S'+1)e^{-E(S')/kT}}$$

$$\chi_M = \chi_{M'}(1-\rho) + \frac{4S(S+1)N\beta^2 g^2 \rho}{3kT} + \mathrm{TIP}$$

where ρ is a paramagnetic impurity fraction and TIP is a temperature independent paramagnetism. Using this model, the susceptibility for **1** above 2.0 K was simulated, leading to the values of $J = -0.79$ cm^{-1}, $g = 2.01$, $\rho = 0.013$ and TIP = 418×10^{-6} cm^3 mol^{-1} with $R = 4.80 \times 10^{-6}$ ($R = \sum(\chi_{obs}T - \chi_{calc}T)^2/\sum(\chi_{obs}T)^2$). A negative J parameter confirms a weak antiferromagnetic exchange coupling between the adjacent Ni(II) centers, which is also in agreement with a negative θ value.

Table S1. Selected bond lengths [Å] and angles [°] for compounds **1**–**7**.[a]

1					
Mn(1)-O(2)	2.1665(1)	Mn(1)-O(3)#1	2.1327(1)	Mn(1)-O(7)	2.1796(1)
Mn(1)-N(1)	2.2468(1)	Mn(1)-N(2)	2.3000(1)	Mn(1)-N(3)	2.2463(1)
O(2)-Mn(1)-O(7)	158.43(1)	O(2)-Mn(1)-N(1)	74.42(1)	O(2)-Mn(1)-N(2)	111.31(1)
O(2)-Mn(1)-N(3)	92.45(1)	O(2)-Mn(1)-O(3)#1	92.68(1)	O(7)-Mn(1)-N(1)	87.91(1)
O(7)-Mn(1)-N(2)	82.13(1)	O(7)-Mn(1)-N(3)	107.93(1)	O(3)#1-Mn(1)-O(7)	81.56(1)
N(1)-Mn(1)-N(2)	95.50(1)	N(1)-Mn(1)-N(3)	158.55(1)	O(3)#1-Mn(1)-N(1)	109.71(1)
N(2)-Mn(1)-N(3)	73.18(1)	O(3)#1-Mn(1)-N(2)	149.27(1)	O(3)#1-Mn(1)-N(3)	87.38(1)
2					
Mn(1)-O(1)	2.2005(2)	Mn(1)-O(4)#1	2.1899(2)	Mn(1)-O(7)	2.2436(2)
Mn(1)-N(1)	2.2805(2)	Mn(1)-N(2)	2.2926(2)	Mn(1)-N(5)	2.2362(2)
O(1)-Mn(1)-O(7)	88.37(1)	O(1)-Mn(1)-N(1)	73.43(1)	O(1)-Mn(1)-N(2)	97.75(1)
O(1)-Mn(1)-N(5)	90.69(1)	O(1)-Mn(1)-O(4)#1	150.29(1)	O(7)-Mn(1)-N(1)	97.80(1)
O(7)-Mn(1)-N(2)	161.19(1)	O(7)-Mn(1)-N(5)	87.00(1)	O(4)#1-Mn(1)-O(7)	76.65(1)
N(1)-Mn(1)-N(2)	100.99(1)	N(1)-Mn(1)-N(5)	163.18(1)	O(4)#1-Mn(1)-N(1)	83.24(1)
N(2)-Mn(1)-N(5)	75.21(1)	O(4)#1-Mn(1)-N(2)	104.66(1)	O(4)#1-Mn(1)-N(5)	113.58(1)
3					
Ni(1)-O(2)	2.0275(2)	Ni(1)-N(1)	2.0855(2)	Ni(1)-N(2)	2.0783(2)
Ni(1)-N(3)	2.0742(2)	Ni(1)-N(4)	2.0892(2)	Ni(1)-N(5)	2.0696(2)
O(2)-Ni(1)-N(1)	79.70(1)	O(2)-Ni(1)-N(2)	88.44(1)	O(2)-Ni(1)-N(3)	92.85(1)
O(2)-Ni(1)-N(4)	168.93(1)	O(2)-Ni(1)-N(5)	91.47(1)	N(1)-Ni(1)-N(2)	166.12(1)
N(1)-Ni(1)-N(3)	93.85(1)	N(1)-Ni(1)-N(4)	93.15(1)	N(1)-Ni(1)-N(5)	87.87(1)

N(2)-Ni(1)-N(3)	79.46(1)	N(2)-Ni(1)-N(4)	99.60(1)	N(2)-Ni(1)-N(5)	99.71(1)
N(3)-Ni(1)-N(4)	96.08(1)	N(3)-Ni(1)-N(5)	175.57(1)	N(4)-Ni(1)-N(5)	79.74(1)
4					
Ni(1)-O(1)	2.0868(1)	Ni(1)-O(2)#1	2.0157(1)	Ni(1)-O(7)	2.0630(1)
Ni(1)-N(1)#1	2.0863(1)	Ni(1)-N(2)	2.0920(1)	Ni(1)-N(3)	2.1068(1)
O(1)-Ni(1)-O(7)	103.00(1)	O(1)-Ni(1)-N(2)	88.47(1)	O(1)-Ni(1)-N(3)	89.19(1)
O(1)-Ni(1)-O(2)#1	82.30(1)	O(1)-Ni(1)-N(1)#1	162.16(1)	O(7)-Ni(1)-N(2)	93.68(1)
O(7)-Ni(1)-N(3)	87.01(1)	O(2)#1-Ni(1)-O(7)	172.97(1)	N(2)-Ni(1)-N(3)	94.82(1)
O(2)#1-Ni(1)-N(2)	91.05(1)	N(1)#1-Ni(1)-N(2)	91.31(1)	O(2)#1-Ni(1)-N(3)	88.48(1)
N(1)#1-Ni(1)-N(3)	90.87(1)	O(2)#1-Ni(1)-N(1)#1	79.86(1)		
5					
Cu(1)-O(1)	2.8686(2)	Cu(1)-O(2)	1.9924(2)	Cu(1)-N(4)	2.0298(2)
Cu(1)-N(5)	1.9915(2)	Cu(1)-N(6)	2.1919(2)	Cu(1)-N(7)	2.0157(2)
Cu(2)-O(6)	1.9564(2)	Cu(2)-O(7)	1.9841(2)	Cu(2)-O(12)	2.3060(2)
Cu(2)-N(1)	1.9498(2)	Cu(2)-N(2)	1.9666(2)	Cu(3)-O(9)	1.9623(2)
Cu(3)-O(10)	2.8463(2)	Cu(3)-N(8)	2.2034(2)	Cu(3)-N(9)	2.0147(2)
Cu(3)-N(10)	1.9946(2)	Cu(3)-N(11)	2.0448(2)	Cu(4)-O(13)	1.9274(2)
Cu(4)-O(13)#1	1.9274(2)	Cu(4)-O(15)#2	2.7500(2)	Cu(4)-O(15)#3	2.7500(2)
Cu(4)-N(3)	1.9822(2)	Cu(4)-N(3)#1	1.9822(2)		
O(1)-Cu(1)-O(2)	49.94(1)	O(1)-Cu(1)-N(4)	103.24(1)	O(1)-Cu(1)-N(5)	97.62(1)
O(1)-Cu(1)-N(6)	138.15(1)	O(1)-Cu(1)-N(7)	84.80(1)	O(2)-Cu(1)-N(4)	152.29(1)
O(2)-Cu(1)-N(5)	93.64(1)	O(2)-Cu(1)-N(6)	91.24(1)	O(2)-Cu(1)-N(7)	89.85(1)
N(4)-Cu(1)-N(5)	82.20(1)	N(4)-Cu(1)-N(6)	116.47(1)	N(4)-Cu(1)-N(7)	94.81(1)
N(5)-Cu(1)-N(6)	100.18(1)	N(5)-Cu(1)-N(7)	176.50(1)	N(6)-Cu(1)-N(7)	79.50(1)
O(6)-Cu(2)-O(7)	159.97(1)	O(6)-Cu(2)-O(12)	94.13(1)	O(6)-Cu(2)-N(1)	83.94(1)
O(6)-Cu(2)-N(2)	94.18(1)	O(7)-Cu(2)-O(12)	105.82(1)	O(7)-Cu(2)-N(1)	93.45(1)
O(7)-Cu(2)-N(2)	82.97(1)	O(12)-Cu(2)-N(1)	101.84(1)	O(12)-Cu(2)-N(2)	93.85(1)
N(1)-Cu(2)-N(2)	164.29(1)	O(9)-Cu(3)-O(10)	50.57(1)	O(9)-Cu(3)-N(8)	96.17(1)
O(9)-Cu(3)-N(9)	90.88(1)	O(9)-Cu(3)-N(10)	96.08(1)	O(9)-Cu(3)-N(11)	162.66(1)
O(10)-Cu(3)-N(8)	146.65(1)	O(10)-Cu(3)-N(9)	101.16(1)	O(10)-Cu(3)-N(10)	84.85(1)
O(10)-Cu(3)-N(11)	112.10(1)	N(8)-Cu(3)-N(9)	78.84(1)	N(8)-Cu(3)-N(10)	98.39(1)
N(8)-Cu(3)-N(11)	101.17(1)	N(9)-Cu(3)-N(10)	172.77(1)	N(9)-Cu(3)-N(11)	92.61(1)
N(10)-Cu(3)-N(11)	81.33(1)	O(13)-Cu(4)-N(3)#1	95.50(1)	O(15)#2-Cu(4)-N(3)	94.61(1)
O(15)#3-Cu(4)-N(3)	85.39(1)	O(13)#1-Cu(4)-O(15)#2	97.01(1)	O(13)#1-Cu(4)-O(15)#3	82.99(1)
O(13) -Cu(4)-N(3)	84.50(1)				
6					
Ni(1)-O(2)	2.0705(2)	Ni(1)-O(4)#1	2.0463(2)	Ni(1)-O(5)#1	2.0770(2)
Ni(1)-O(7)	2.0596(2)	Ni(1)-N(1)	2.1262(2)	Ni(1)-N(2)	2.1006(2)
Ni(2)-O(8)	2.0280(2)	Ni(2)-O(8)#2	2.0280(2)	Ni(2)-O(9)	2.0789(2)
Ni(2)-O(9)#2	2.0789(2)	Ni(2)-N(3)	2.1387(2)	Ni(2)-N(3)#2	2.1387(2)
O(2)-Ni(1)-O(7)	94.25(1)	O(2)-Ni(1)-N(1)	78.50(1)	O(2)-Ni(1)-N(2)	87.77(1)
O(2)-Ni(1)-O(4)#1	178.88(1)	O(2)-Ni(1)-O(5)#1	91.87(1)	O(7)-Ni(1)-N(1)	92.28(1)
O(7)-Ni(1)-N(2)	89.09(1)	O(4)#1-Ni(1)-O(7)	86.80(1)	O(5)#1-Ni(1)-O(7)	171.77(1)
N(1)-Ni(1)-N(2)	166.26(1)	O(4)#1-Ni(1)-N(1)	101.09(1)	O(5)#1-Ni(1)-N(1)	94.33(1)
O(4)#1-Ni(1)-N(2)	92.64(1)	O(5)#1-Ni(1)-N(2)	85.65(1)	O(4)#1-Ni(1)-O(5)#1	87.13(1)
O(8)-Ni(2)-O(9)	90.82(1)	O(8)-Ni(2)-N(3)	86.86(1)	O(8)-Ni(2)-O(9)#2	89.18(1)
O(8)-Ni(2)-N(3)#2	93.14(1)	O(9)-Ni(2)-N(3)	90.95(1)	O(9)-Ni(2)-N(3)#2	89.05(1)
7					
Zn(1)-O(1)	2.1110(1)	Zn(1)-O(3)#1	1.9645(1)	Zn(1)-O(7)	2.0395(1)
Zn(1)-N(2)	2.0901(1)	Zn(1)-N(3)	2.1660(1)	Zn(2)-O(2)	2.3675(1)
Zn(2)-O(2)#3	2.3675(1)	Zn(2)-O(5)#2	2.0353(1)	Zn(2)-O(5)#4	2.0353(1)

Zn(2)-N(1)#2	2.0737(1)				
O(1)-Zn(1)-O(7)	89.80(1)	O(1)-Zn(1)-N(2)	89.74(1)	O(1)-Zn(1)-N(3)	152.23(1)
O(1)-Zn(1)-O(3)#1	99.33(1)	O(7)-Zn(1)-N(2)	148.22(1)	O(7)-Zn(1)-N(3)	87.89(1)
O(3)#1-Zn(1)-O(7)	98.24(1)	N(2)-Zn(1)-N(3)	78.08(1)	O(3)#1-Zn(1)-N(2)	113.17(1)
O(3)#1-Zn(1)-N(3)	108.39(1)	O(2)-Zn(2)-O(5)#2	94.47(1)	O(2)-Zn(2)-N(1)#2	88.33(1)
O(2)-Zn(2)-O(5)#4	85.53(1)	O(2)-Zn(2)-N(1)#4	91.67(1)	O(5)#2-Zn(2)-N(1)#2	80.97(1)
O(2)#2-Zn(2)-N(1)#4	99.03(1)				

[a] Symmetry transformations used to generate equivalent atoms: #1 –*x*+2, –*y*+2, –*z* for **1**; #1 *x*, –*y*+2, *z*+1/2 for **2**; #1 –*x*+3/2, *y*–1/2, –*z*+1/2 for **4**; #1 –*x*+2, –*y*, –*z*+1; #2 –*x*+1, –*y*+1, –*z*+1; #3 –*x*+1, –*y*, –*z*+1 for **5**; #1 –*x*+2, –*y*+1, –*z*+2; #2 –*x*, –*y*, –*z*–1 for **6**; #1 –*x*+1/2, *y*–1/2, –*z*+3/2; #2 *x*, *y*–1, *z*; #3 –*x*+1, –*y*, –*z*+1; #4 –*x*+1, –*y*+1, –*z*+1 for **7**.

Table S2. Hydrogen bonds in crystal packing [Å, °] of **1**–**7**.

Compound	D-H…A	*d*(D-H)	*d*(H…A)	*d*(D…A)	∠DHA	Symmetry code
1	O(4)-H(1)···O(5)	1.32	1.10	2.4226(1)	174.00	*x*, *y*, *z*-1
	O(7)-H(1W)···O(6)	0.89	1.89	2.7759(1)	175.00	-*x*+1, -*y*+2, -*z*
	O(7)-H(2W)···O(1)	0.81	1.89	2.6744(1)	166.00	-*x*+1, *y*, *z*
2	O(6)-H(1)···O(1)	0.82	1.82	2.6168(2)	164.00	*x*-1/2, *y*+1/2, *z*-1
	O(7)-H(1W)···O(8)	0.86	1.92	2.7013(3)	150.00	*x*+1/2, -*y*+3/2, *z*+1/2
	N(3)-H(2)···O(3)	0.86	1.92	2.7363(3)	159.00	*x*, *y*, *z*+1
	O(7)-H(2W)···O(2)	0.87	1.94	2.8023(3)	173.00	*x*, *y*+1, *z*
	O(8)-H(3W)···O(3)	0.85	2.01	2.8323(3)	163.00	*x*, -*y*+1, *z*+1/2
	N(4)-H(4)···O(4)	0.86	2.01	2.8639(3)	169.00	*x*, *y*, *z*+1
	O(8)-H(4W)···O(5)	0.85	2.13	2.9587(3)	167.00	*x*, -*y*+2, *z*+1/2
3	O(4)-H(1)···O(5)	1.09	1.29	2.3778(3)	174.00	
	O(7)-H(1W)···O(8)	0.85	2.31	2.8343(3)	120.00	
	O(7)-H(2W)···O(9)	0.84	1.84	2.6851(3)	178.00	-*x*+3/2, *y*+1/2, -*z*+1/2
	O(8)-H(3W) ···O(1)	0.85	1.97	2.8178(3)	179.00	
	O(8)-H(4W) ···O(6)	0.85	1.89	2.7429(3)	179.00	*x*+1, *y*, *z*
	O(9)-H(5W) ···O(2)	0.86	1.94	2.7947(3)	179.00	
	O(9)-H(6W) ···O(3)	0.85	1.89	2.7354(3)	179.00	-*x*+1, -*y*+1, -*z*
	O(10)-H(7W) ···O(7)	0.73	1.82	2.5451(3)	173.00	
4	O(5)-H(1)···O(4)	0.82	1.57	2.3903(1)	174.00	
	O(7)-H(1W)···O(6)	0.86	1.92	2.6496(1)	142.00	*x*+1/2, -*y*+5/2, *z*-1/2
	O(7)-H(2W)···O(2)	0.86	1.99	2.6872(1)	138.00	
5	O(4)-H(1)···O(8)	0.83	1.78	2.6091(2)	172.00	-*x*-1, -*y*+1, -*z*
	O(16)-H(2)···O(18)	0.82	1.56	2.3752(2)	170.00	
	O(19)-H(2W)···O(13)	0.85	2.19	2.9405(2)	148.00	-*x*+2, -*y*, -*z*+1
	O(20)-H(3W)···O(21)	0.85	1.93	2.7470(2)	161.00	
	O(21)-H(5W)···O(11)	0.85	1.87	2.7243(2)	179.00	*x*+1, *y*, *z*
	O(21)-H(6W)···O(18)	0.85	1.87	2.7179(2)	179.00	*x*+1, *y*, *z*
	O(22)-H(7W)···O(10)	0.85	2.09	2.9369(2)	179.00	
	O(22)-H(8W)···O(17)	0.85	1.89	2.7415(2)	178.00	
	O(23)-H(9W)···O(22)	0.81	2.28	2.9589(2)	141.00	
	O(23)-H(10W)···O(12)	0.84	2.07	2.8550(2)	155.00	
6	O(7)-H(1W)···O(6)	0.86	1.93	2.7340(2)	157.00	-*x*+3, -*y*+1, -*z*+2
	O(7)-H(2W)···O(2)	0.85	1.97	2.8184(2)	180.00	-*x*+2, -*y*+1, -*z*+1
	O(8)-H(3W)···O(10)	0.86	2.01	2.6900(2)	136.00	*x*, *y*, *z*-1
	O(8)-H(4W)···O(4)	0.89	1.89	2.6919(2)	149.00	-*x*+1, -*y*+1, -*z*+1
	O(9)-H(5W)···O(3)	0.87	1.81	2.6773(2)	172.00	-*x*+1, -*y*+1, -*z*+1
	O(9)-H(6W)···O(10)	0.87	2.05	2.8608(2)	153.00	-*x*, -*y*, -*z*
	O(10)-H(7W)···O(5)	0.85	2.15	2.9758(2)	165.00	-*x*+2, -*y*+1, -*z*+2
	O(10)-H(8W)···O(1)	0.97	1.77	2.7398(2)	172.00	-*x*+2, -*y*+1, -*z*+2
	O(11)-H(9W)···O(6)	0.85	1.99	2.8347(2)	178.00	-*x*+1, -*y*+1, -*z*+1
7	O(7)-H(1W)···O(9)	0.76	1.95	2.6624(1)	156.00	-*x*+1, -*y*, -*z*+1
	O(7)-H(2W)···O(2)	0.85	1.76	2.6152(1)	180.00	
	O(8)-H(3W)···O(6)	0.80	2.03	2.8254(1)	174.00	-*x*+1/2, *y*-1/2, -*z*+1/2

O(8)-H(4W)···O(4)	0.76	2.11	2.7763(1)	146.00	-*x*+1, -*y*+1, -*z*+1
O(9)-H(5W)···O(5)	0.87	2.00	2.7770(1)	150.00	*x*, *y*-1, *z*
O(9)-H(6W)···O(8)	0.86	1.85	2.7034(1)	173.00	

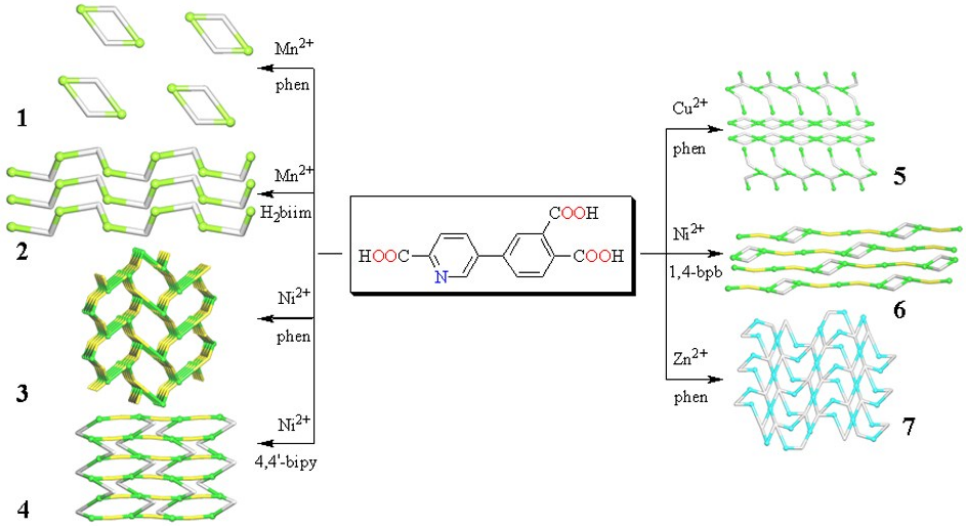

Scheme S1. Illustration of the effect of metal(II) nodes and supporting ligands on the topology of compounds **1**–**7**.

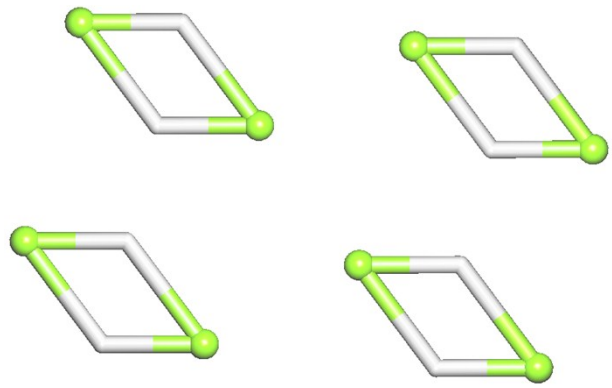

Fig. S1. Topological representation of discrete underlying Mn_2 units with the **1M2-1** topology in **1**. Color codes: Mn centers (lime green balls), centroids of μ-$Hdppa^{2-}$ units (gray).

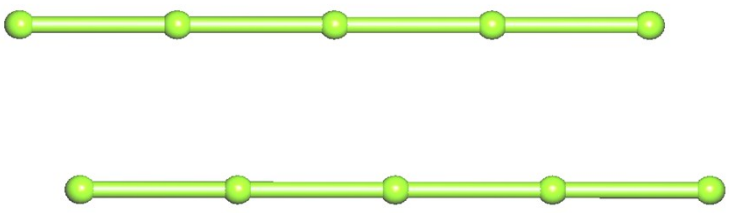

Fig. S2. Topological representation of linear 1D H-bonded underlying chains with the **2C1** topology in **1**. Color code: centroids of $[Mn_2(\mu\text{-}Hdppa)_2(phen)_2(H_2O)_2]$ molecular units (lime green balls).

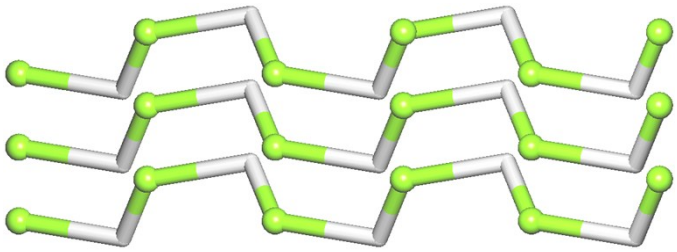

Fig. S3. Topological representation of the interdigitated zigzag 1D chains displaying a uninodal 2-connected underlying net with the **2C1** topology in **2**. View along the *a* axis; color codes: Mn centers (lime green balls), centroids of μ-Hdppa^{2-} linkers (gray).

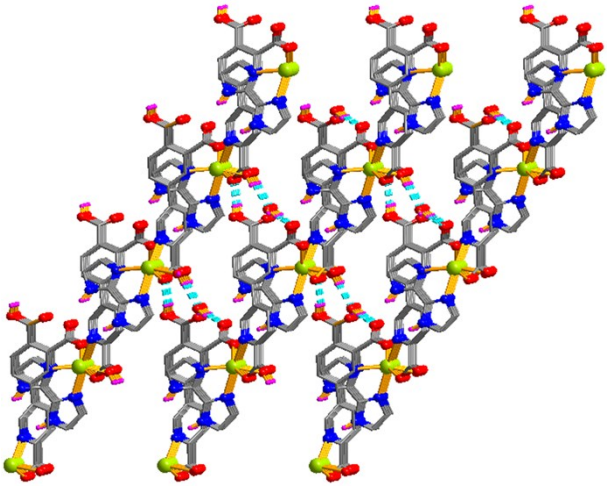

Fig. S4. 3D supramolecular net in **2** seen along the *b* axis (blue lines present the H-bonds).

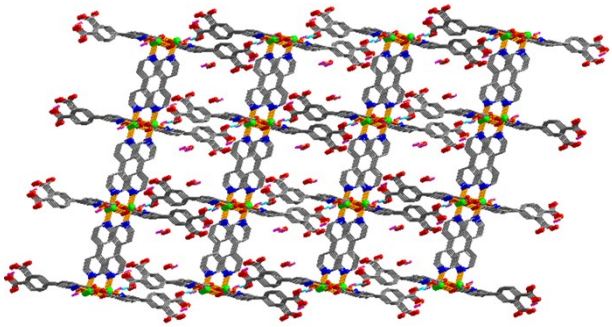

Fig. S5. 3D supramolecular net in **4** seen along the *b* axis (blue lines present the H-bonds).

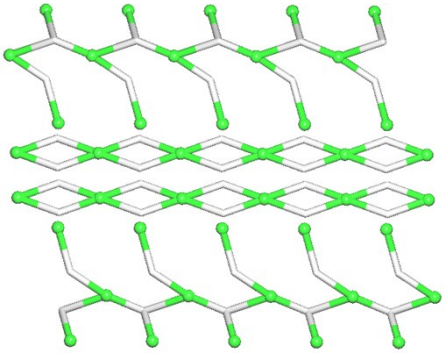

Fig. S6. Topological representation of the underlying network displaying two types of the decorated uninodal 2-connected chains with the **2C1** topology in **5**. Rotated view along the *b* axis; color codes: Cu centers (green balls), centroids of μ_3-dppa^{3-}/μ-Hdppa^{2-} linkers (gray).

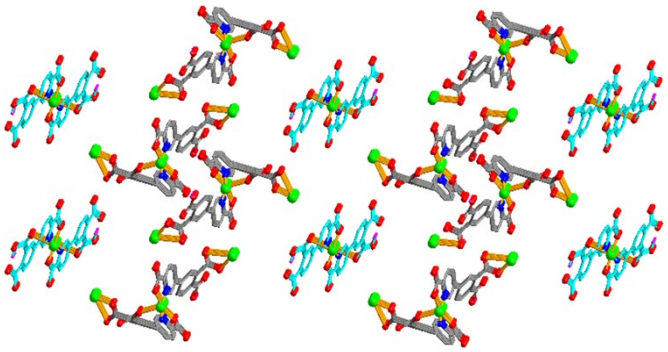

Fig. S7. Two different types of 1D metal-organic chains in **5** seen along the *a* axis.

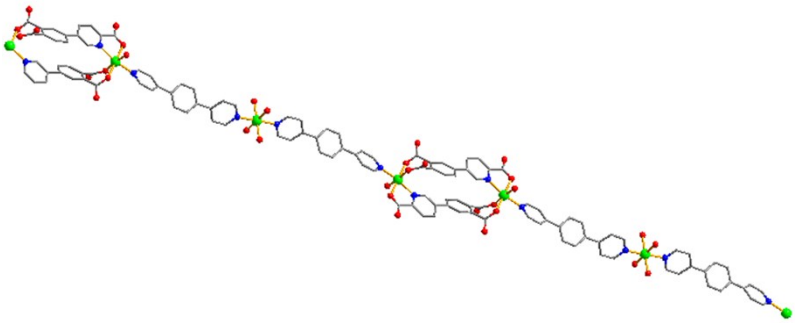

Fig. S8. 1D metal-organic chain in **6** seen along the *b* axis.

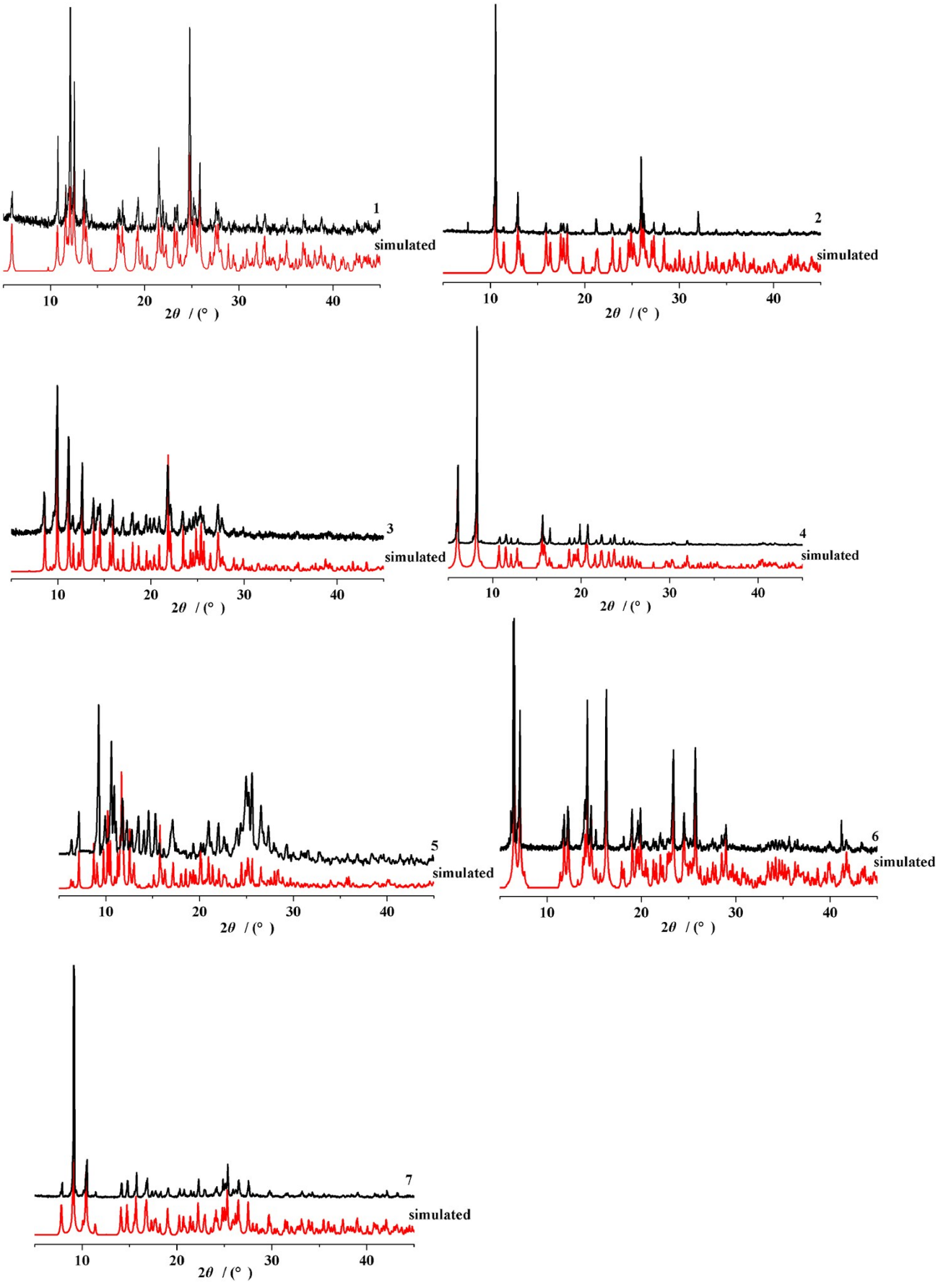

Fig. S9. Experimental and simulated PXRD patterns of compounds **1**–**7** at room temperature.

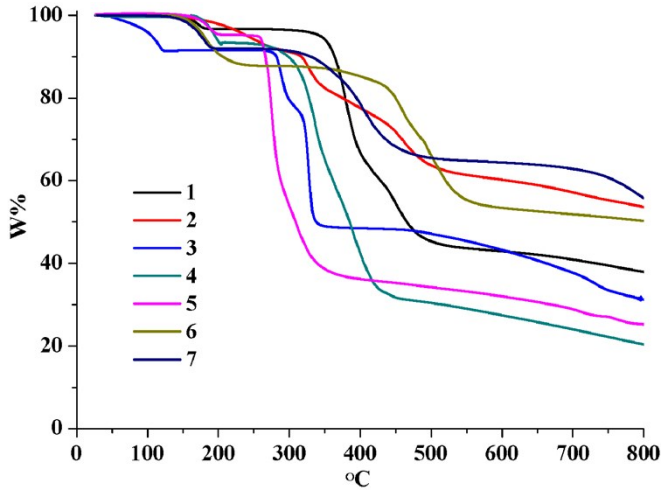

Fig. S10. Thermogravimetric analysis (TGA) curves of compounds **1**–**7**.

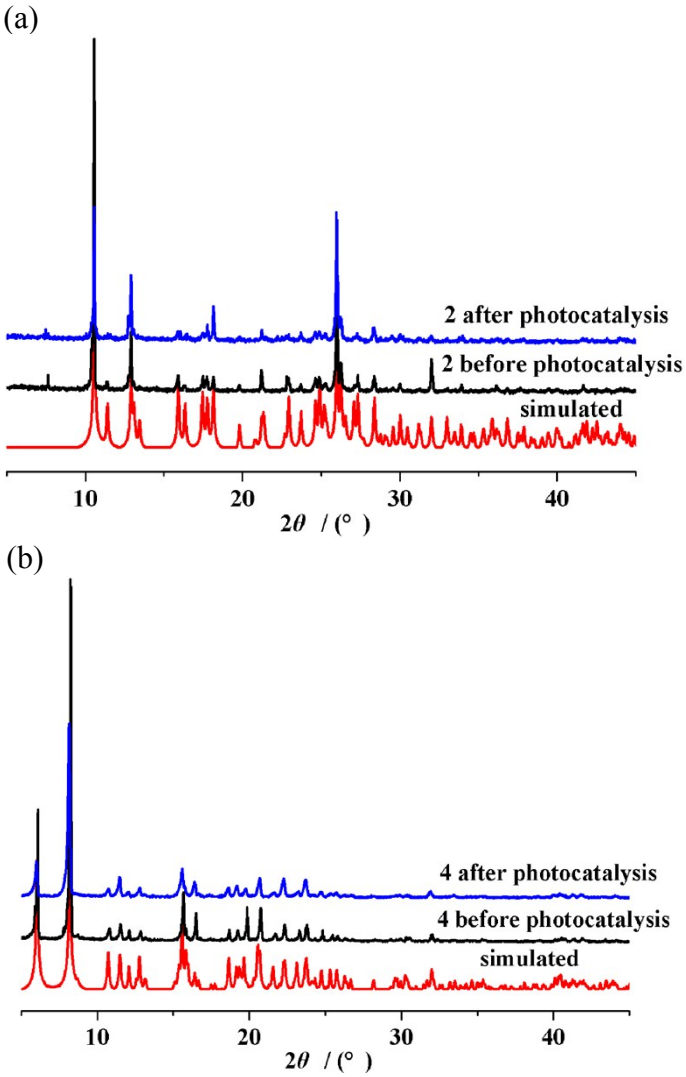

Fig. S11. PXRD patterns for **2** (a) and **4** (b): simulated (red), before photocatalysis (black), and after photocatalytic experiments (blue).

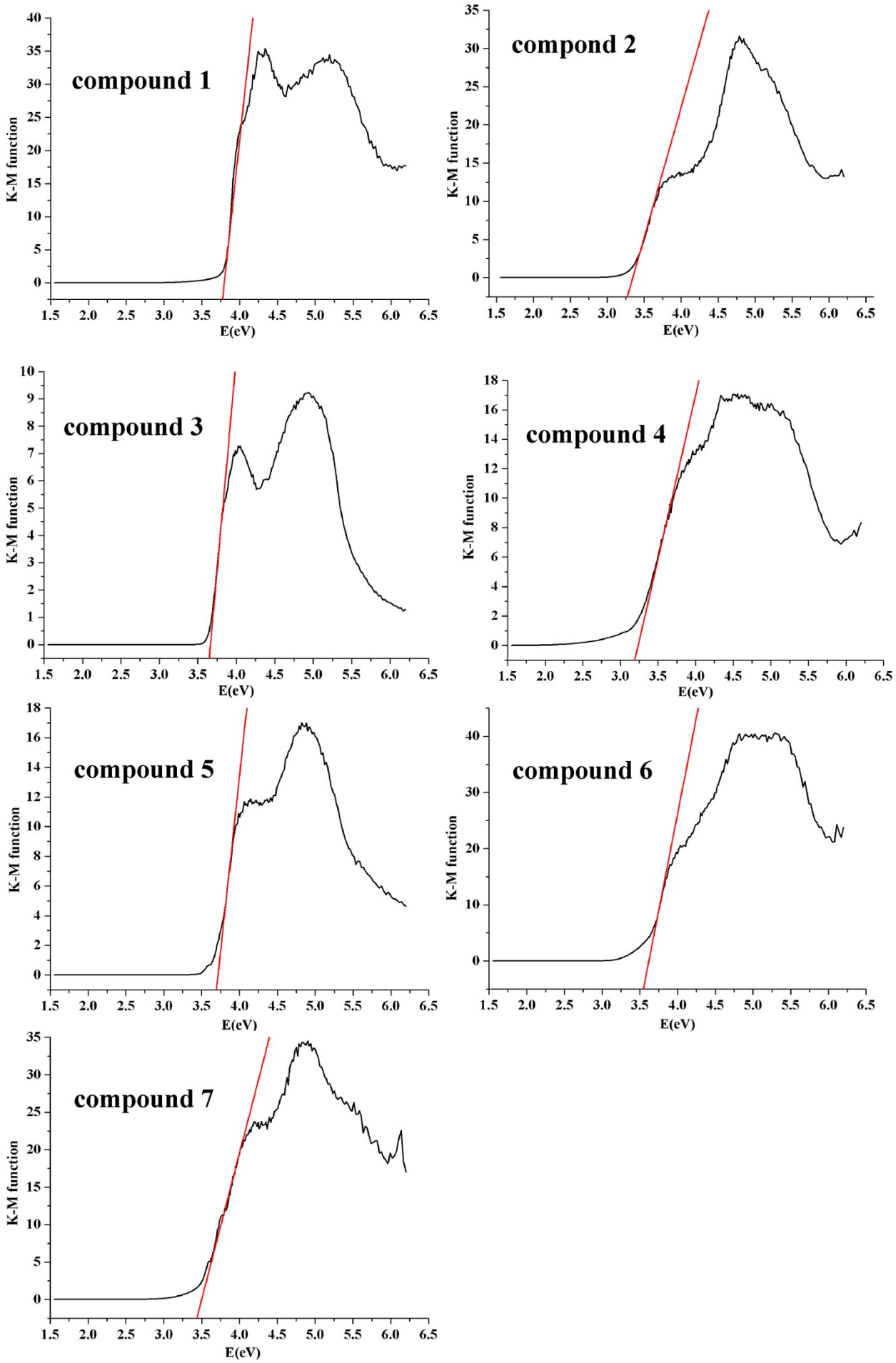

Fig. S12. Kubelka-Munk-transformed diffuse reflectance spectra of compounds **1**–**7**.

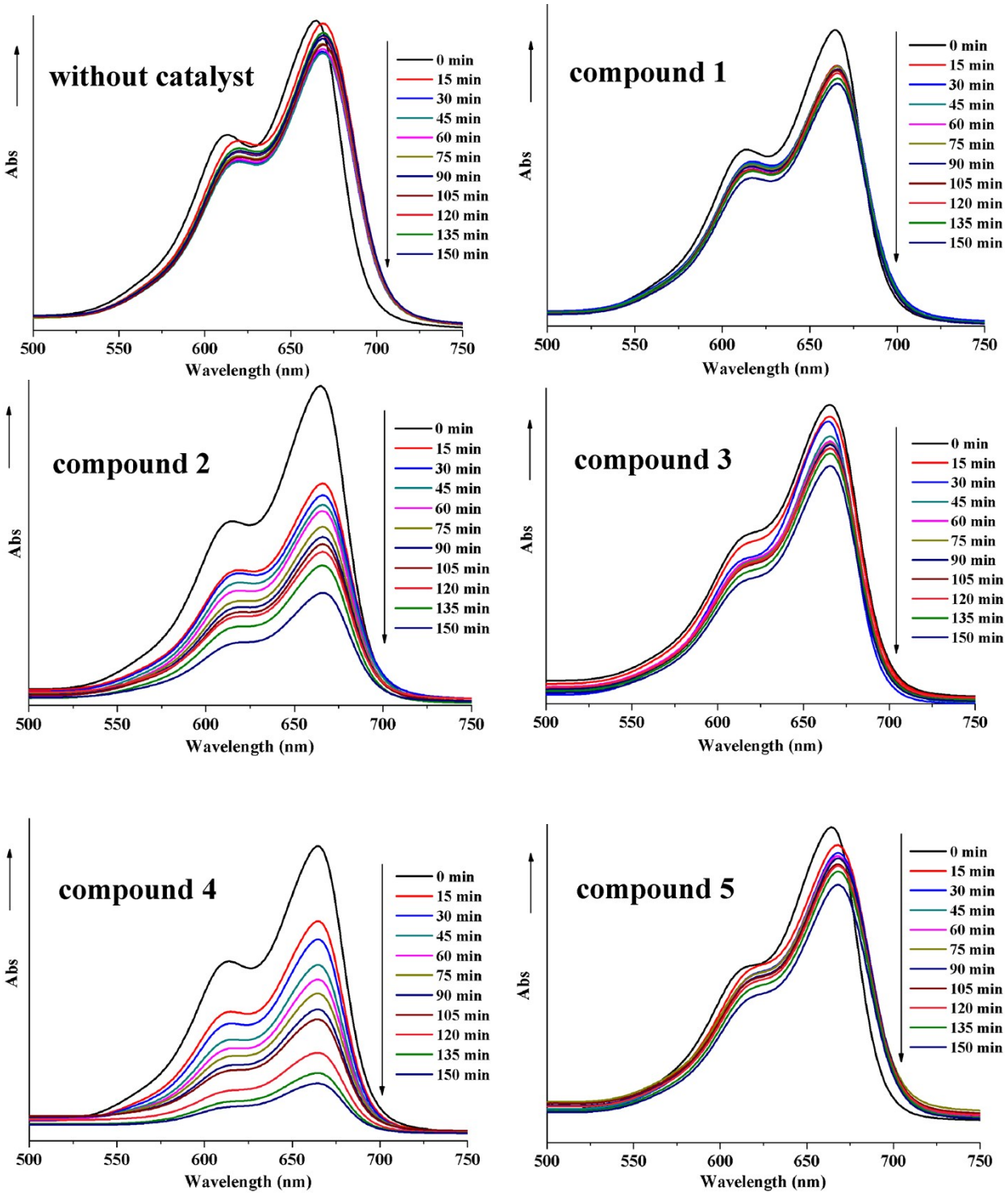
without catalyst
compound 1
compound 2
compound 3
compound 4
compound 5
Abs
Wavelength (nm)
500
550
600
650
700
750
0 min
15 min
30 min
45 min
60 min
75 min
90 min
105 min
120 min
135 min
150 min

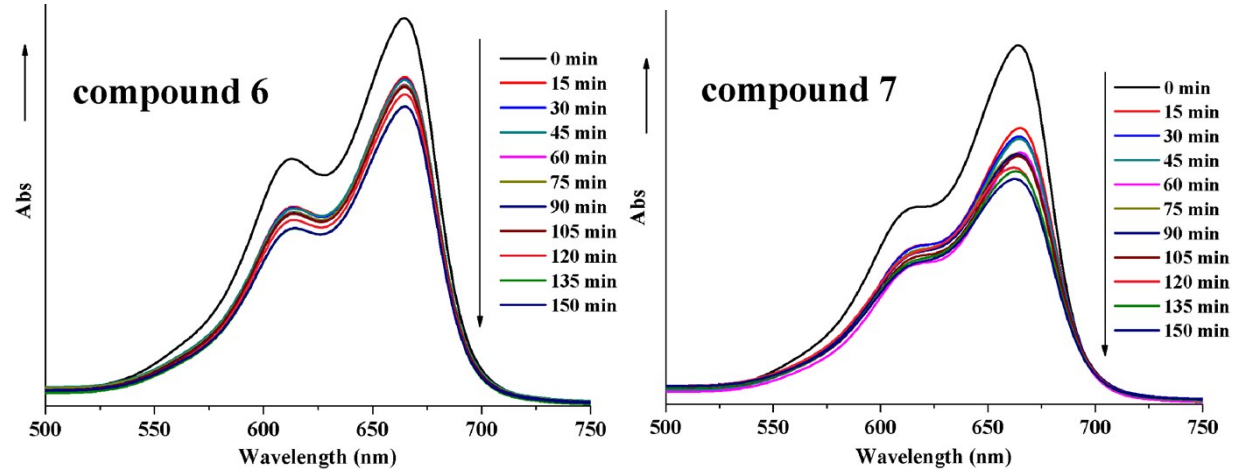

Fig. S13. Time-dependent UV-Vis spectra of the reaction mixtures in the course of the MB photodegradation catalyzed by **1**–**7** (blank test in the abcence of catalyst is included for comparison). Reaction conditions: catalyst (50 mg), 100 mL aqueous solution, MB (1 mg) under 125 W Hg lamp irradiation.

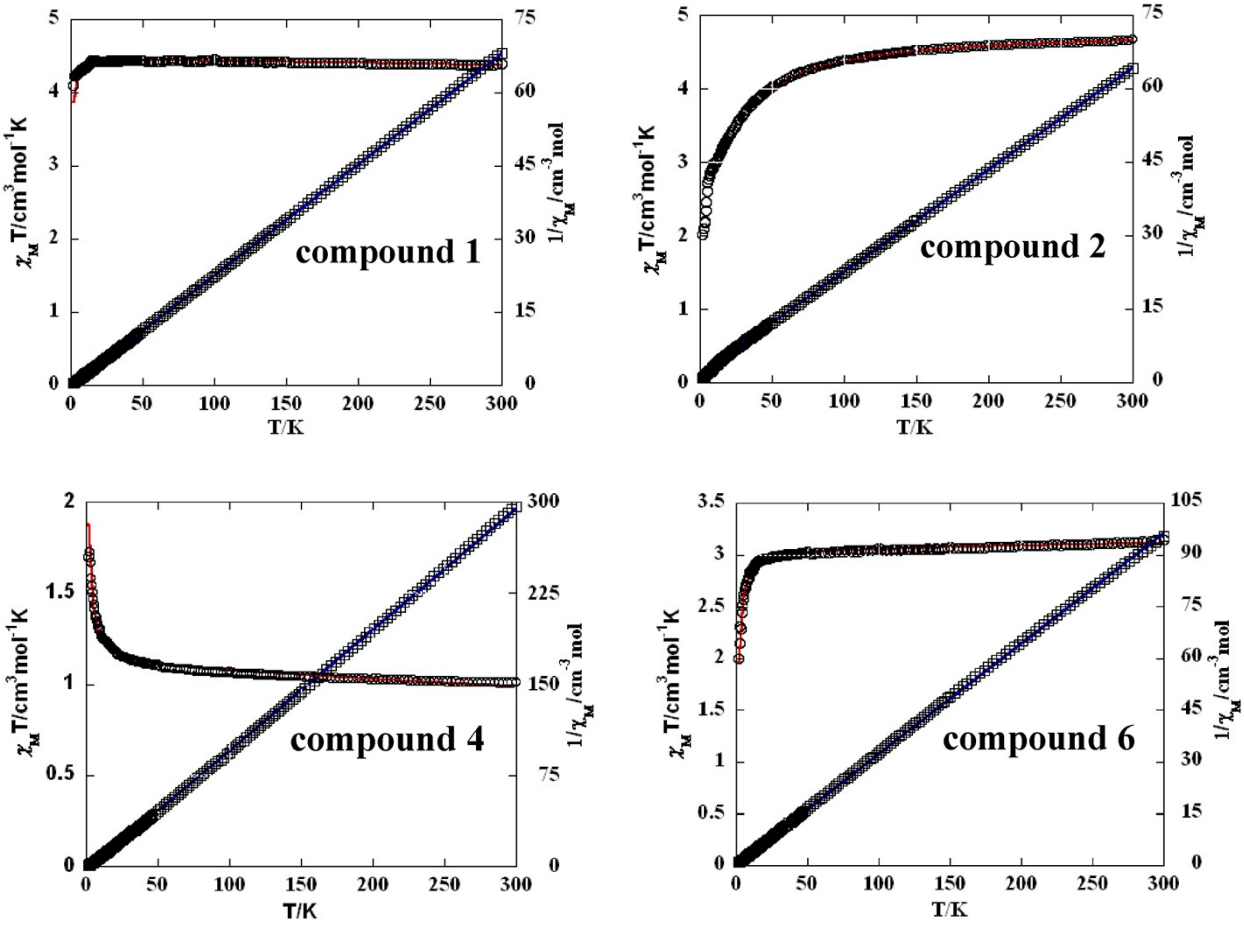

Fig. S14. Temperature dependence of $\chi_M T$ (O) and $1/\chi_M$(□) vs. T for compounds **1**, **2**, **4**, and **6**. The red lines represent the best fit to the equations in the text. The blue lines show the Curie–Weiss fitting.

Supporting references

1 G. M. Yu, L. Zhao, Y. N. Guo, G. F. Xu, L. F. Zou, J. Tang and Y. H. Li, *J. Mol. Struct*., 2010, **982**, 139.

2 W. Hiller, J. Strähel, A. Datz, M. Hanack, W. E. Hatfield, L. W. Ter Haar and P. Gütlich, *J. Am. Chem. Soc.*, 1984, **106**, 329.

3 L. H. Jia, R. Y. Li, Z. M. Duan, S. D. Jiang, B. W. Wang, Z. M. Wang and S. Gao, *Inorg. Chem.*, 2011, **50**, 144.

4 O. Kahn, *Molecular Magnetism*, VCH, New York, 1993.

5 C. Y. Weng, *Thesis*, Carnegie Mellon University, Pittsburgh, PA, 1969.

6 L. K. Thompson, V. Niel, H. Grove, D. O. Miller, M. J. Newlands, P. H. Bird, W. A. Wickramasinghe and A. B. P. Lever, *Polyhedron*, 2004, **23**, 1175.